A comprehensive techno-eco-assessment of CO_2 enhanced oil recovery projects using a machine-learning assisted workflow

Junyu You[1,2], William Ampomah[2*], Anthony Morgan[2], Qian Sun[2,3], Xiaoliang Huang[1]

1 College of Petroleum and Natural Gas Engineering, Chongqing University of Science and Technology, Chongqing, 401331, China

2 Petroleum Recovery Research Center, New Mexico Tech, Socorro NM, 87801, USA

3 Department of Energy Resource, China University of Geoscience, Beijing, 100083, China

Keywords

CCUS, CO_2-EOR, multi-objective optimization, economics assessment, machine learning

Abstract

Carbon dioxide enhanced oil recovery (CO_2-EOR) projects not only extract residual oil but also sequestrate CO_2 in the depleted reservoirs. This study develops a machine-learning-based workflow to co-optimize the hydrocarbon recovery, CO_2 sequestration volume and project net present value (NPV) simultaneously. Considering the trade-off relationships amongst the objective functions, support vector regression with Gaussian kernel (Gaussian- SVR) proxies are coupled with multi-objective particle swarm optimization (PSO) protocol and generate Pareto optimal solutions. Taking advantage of the high computational efficacy of the proxy model, economic uncertainties introduced by tax credits, capital costs and oil price are investigated by this study. The results indicate that the tax incentive policy (Section 45Q) plays a vital role in enhancing the economic returns of CO_2-EOR projects, especially under the depression of crude oil market. The proposed workflow has been successfully implemented to optimize a water alternative CO_2

(CO_2−WAG) injection project in a depleted oil sand in the US. The optimization results yield an incremental oil production of 15.8 MM STB and 1.37 MM metric tons of CO_2 storage in a 20-year development strategy, with the highest project NPV to be 205.6 MM US dollars.

1. Introduction

Geological long-term CO_2 sequestration is a critical technology to reduce CO_2 emission and mitigate global warning[1-3]. In the oil and gas industry, CO_2-EOR extracts residual oil from mature oil fields by injecting CO_2. Meanwhile, the injected CO_2 could be sequestered in the depleted porous media. Thus, CO_2-EOR is seen as an cost-effective means to implement the geological storage of anthropogenic CO_2.[1] Such a kind of project is known to be Carbon Capture, Utilization and Storage (CCUS) project.

The United States Department of Energy (U.S. DOE) funded the Southwest Regional Partnership on Carbon Sequestration (SWP), which has been monitoring a water-alternating-CO_2 injection (CO_2-WAG) project at the Farnsworth Unit Field (FWU) in Ochiltree County, Texas[3]. The primary goals of the SWP project include monitoring the injection of over one million metric tons of anthropogenic CO_2, investigating the migration of CO_2 plume, and studying how to store CO_2 in the partially depleted oil and gas reservoirs safely and permanently. [2-6]

The implementation of safe and long-term sequestration of CO_2 in subsurface structure is the main concern of the studies on CCUS projects. Numerous researches have been carried out on the mechanisms of the CO_2 trapping, including structural-stratigraphic trapping[6], solubility trapping[7],

residual trapping[8], and mineral trappings [9, 10]. More importantly, factors related with the performance of CO_2 storage gains a lot of attention recently, such as three-phase hysteresis [8], the impacts of heterogeneity[11, 12], formation fluid dissolved components [13], and CO_2 injectivity[14], etc. For a CCUS project, the field operator seeks to optimize multiple objectives simultaneously, including oil recovery, carbon storage volume and project economic outcomes. Considering the operational parameters of numerous injection and production wells, the field development strategy design can be recognized as a high-dimensional, multi-objective optimization problem (MOP). Research efforts have been donated to solve MOPs in oil and gas industry: Guevara et al. [15] presented a nonlinear model-based, adaptive-predictive control approach to co-optimize both steam conformance and net present value (NPV). Forooghi et al. [16] employed a compositional reservoir simulator to co-optimize CO_2 sequestration and CO_2-EOR performance in a North Sea chalk field. Han et al. [17] used a multi-objective evolutionary algorithm (MOEA) for history matching with four objective functions. Dai et al.[18] proposed an integrated Monte Carlo simulation framework to optimize the net CO_2 injection and oil recovery after five years in a CO_2-EOR project.

When dealing with MOPs, a commonly used approach is to develop and optimize an aggregated function by weighted summing various objectives,[16, 17, 19] which is known as the Weighted Sum Method (WSM). The main advantage of the WSM is that the combination of multiple objectives reduces the number of objectives functions and the computational overhead. However, defining the magnitudes of the associated weights could be challenging due[20]. More importantly, using

WSM can only find a unique optimal solution, which constrains the flexibility for decision-makers to design a project with multiple objective functions.[21] In petroleum industry, multiple project responses can be combined into the calculation of NPV, then the MOP is converted to a single-objective optimization problem. For example, Wang et al. [22] studied the economic co-optimization of oil recovery and CO_2 sequestration using a method introduced by Leach.[23] Their work focuses on optimizing the project NPV considering different economic components, including CO_2 sequestration subsidies. Omran et al. [20] introduced work to evaluate the economics in a petrochemical production project, focusing on four key factors: capital investments, operating costs, cash flow and profitability measures. However, using this method would encounter the same drawbacks as that of WSM to solve multi-objective problems.

The Pareto optimal theory is an alternative approach to address MOPs, which structures a solution repository (called Pareto front) containing multiple solutions for the objective functions exhibiting trade-off relationship (namely, the improvement of one of the objectives has to sacrifice at least another one). The structure of Pareto fronts would employ an optimization algorithm such as genetic algorithm (MOGA) and particle swarm optimization (MOPSO). Successfully applications of Pareto optimal theory can be found in research areas such as history matching,[24] field development optimization [25] and production performance optimization.[26] The design of CO_2-EOR is extremely suitable to deploy the Pareto optimal theory due to the strong trade-off relationship amongst the objective functions: the maximization of oil recovery would increase the production of CO_2 gas, which reduces the volume of CO_2 residing in the porous media. Moreover, the impact of

the tax subsidies on the project NPV needs to be investigated. Notably, the multiple-objective optimizers are computationally intensive due to the massive volume calculation and sorting of the objective functions, which motivates the use of machine-learning proxies.

In this work, a field-scale numerical simulation model is employed to assess the long-term responses of the CO_2-WAG project. To reduce the computational overhead of such applications, machine-learning models have been trained and acted as proxies of the high-fidelity numerical model to predict specific outcomes[27]. In the petroleum industry, machine-learning models such as Response Surface, Artificial Neural Network (ANN), Support Vector Regression, and Multivariate splines have been employed to solve various regression and classification problems[28-35]. This study develops a machine-learning-assisted workflow coupling Gaussian-SVR and MOPSO to co-optimize the oil recovery, carbon sequestration volume and project NPV. It is employed to conduct a comprehensive techno-eco-assessment of the FWU CO_2-WAG project considering vital economic parameters including the oil price, tax credits, carbon capture and transporting costs, field operational cost, etc. The major contributions of this work are as follows:

An iterative protocol is proposed to reduce the uncertainty introduced by the error margin of the proxy. New samples are added to the dataset and retrain the SVR model until the disparities between the Pareto front generated by the proxy and the numerical simulator satisfy a prescribed tolerance. Moreover, extensive uncertainty analysis is carried by taking advantage of the computational efficacy of the proposed workflow, which brings comprehensive techno-economic insights on the variation of project response with the change of economic factors.

2. Geological Model and History-matching

FWU is a partially depleted oil reservoir undergoing CO_2-WAG injection processes. The target reservoir is the Pennsylvanian-age Morrow B sandstone formation located at a depth between 7550 ft and 7950 ft. The formation has an average dip of less than one degree [6] and was deposited in the late Pennsylvanian by a fluvial system in an incised valley [36]. The initial oil in place (OOIP) and gas initially in place (GIIP) are approximately 120MM barrels and 41.48 Bscf [37]. Table 1 summarizes some crucial properties of the FWU field.

Table 1 Important properties of FUW field

Property	Value	Unit
OOIP	120	MM barrel
GIIP	41.48	BCF
Net pay thickness	22-54	Ft
Initial reservoir pressure	2203	Psi
Initial bubble point pressure	2059	Psi
Reservoir temperature @7900 ft	168	˚F
Mean porosity	14.6%	percentage
Mean permeability	58	mD

A 3-D compositional numerical reservoir simulation model is established to investigate the fluid transportation dynamic of FWU using Eclipse simulator[38]. The simulation is presumed to only consider the effects of structural trapping, solubility trapping and residual trapping. The mineral trapping mechanism is not considered in the simulation since it often takes years to occur and its impact on CO2 storage would be observed on a very long time scale [39].

A compositional geological model has been built and incorporated with the history field data collected up to 2019. The numerical model is validated via a rigorous history matching study using

55 years of primary and secondary (water flooding) recovery data, and nine years of CO_2-WAG data (shown in Figure A- 1 in Appendices). Rose-Coss et al. [40, 41] established eight hydraulic flow units (HFUs) to characterize hydrogeologic heterogeneity for the Morrow B using well log and petrophysical data obtained from various scientific wells with the Farnsworth Unit field. Rasmussen et al.[42] found it was possible to lump some of the HFUs via an experimental study of brine-oil and CO_2-oil core-flooding experiments. Each HFU is characterized using a unique permeability-porosity relationship, which is used to populate the spatial distribution of permeability of the simulation model. Moreover, the three-phase relative permeability characterization varies with the HFU distribution. Therefore, the history-matching process of the FWU field becomes even more challenging due to the high dimensionality of the uncertain petrophysical properties.

This history-matched work is accomplished using a machine-learning-assisted workflow [43]. The tuning parameters used include the permeability multipliers along with the lateral and vertical directions, and the Corey's three-phase relative permeability coefficients

3. Forecasting Scenario and objective functions

The forecasting scenario is structured based on the history-matched model to forecast the field responses of a 20-years CO_2-WAG project (from 2019-12-31 to 2038-1-1). More importantly, it can be employed to optimize the development plan considering the prescribed objective functions.

To control the development plan more efficiently and practically, the whole development plan has

been split into eight time periods in total for more detailed control, as summarized in Table 2.

Table 2. Time schedules of the development plan

Period #	Abbreviation	Start time	End time
1	PD1	2019/12/31	2020/6/30
2	PD2	2020/6/30	2022/1/1
3	PD3	2022/1/1	2023/1/1
4	PD4	2023/1/1	2026/1/1
5	PD5	2026/1/1	2028/1/1
6	PD6	2028/1/1	2030/1/1
7	PD7	2030/1/1	2032/1/1
8	PD8	2032/1/1	2038/01/01

The development strategy includes the injection of purchased CO_2 and recycling CO_2 for reinjection underground. The rate of purchased CO_2 is 8000 Mscf/day from the beginning of the year 2020 and the end of the year 2025. After that, the CO_2 purchasing rate decreases to 6400 Mscf/day by the end of the year 2027. From the year 2028, the CO_2 purchasing rate decreases to 5600 Mscf/day, and this rate will be kept until the end of the year 2029. From 2030, the CO_2 purchasing rate will be reduced to 4800 Mscf/day and will last for another two years. Then, no more CO_2 will be purchased from 2032.

The WAG injectors are divided into four groups, and the WAG wells included in the same group will have the same operational parameters. Based on previous studies and field operator's suggestions[28], some previous producers or unused wells will be converted into WAG wells during the development of the CO_2-WAG project. Those new-proposed WAG injectors will be queued to come on stream based on CO_2 availability and/or project anticipated schedule. The WAG wells were grouped based on their year of operation, location of pattern, and injectivity. The extant

injectors were aligned to come on stream when more CO_2 is produced. It is worth noting that, the schedules of the injectors and producers are based on the strategy as shown in Table 2. The operational parameters are well parameters used to control the injection/production performance of the WAG wells. The total number of operational parameters is 37, which are described in detail in Table A - 1.

The forecasting scenario structures the base case simulation model to assess the objective functions considered in the optimization workflow. The NPV is calculated using a modified equation based on reference[44], expressed as Eq. 1.

$$NPV = -CAPEX + \sum_{i=1}^{n}\left(q_o \times r_o + q_{co2,store} \times r_{co2,credit} - q_{w,inj} \times r_w - q_{w,pro} \times r_{w,pro} - q_{inj,co2} \times r_{co2} - q_{co2,p} \times r_{co2,p}\right)_i \times (1 + r_b)^{-i} \quad \text{(Eq. 1)}$$

where r_o is the oil price after tax and royalty deduction; $r_{co2,credit}$ is the CO_2 storage credit given by the government; $r_{w,inj}$ is the water injection cost; $r_{w,pro}$ is the cost of produced water treatment and recycling; r_{co2} is gas injection cost; $r_{co2,p}$ is the CO_2 purchase price from the plant (including transportation); q_o is oil production at i-th year; $q_{co2,store}$ is CO_2 storage at i-th year; $q_{w,inj}$ is water injection at i-th year; $q_{w,pro}$ is water production at i-th year; $q_{inj,co2}$ is CO_2 injection at i-th year; $q_{co2,p}$ is CO_2 purchased at i-th year; r_b is inflation rate; and $CAPEX$ is Capital expenditure. Subscript i is the index of year.

The values of those economic parameters used to calculate the NPV for the base case model are shown in Table 3. The values are extracted from the published references. [44]

Table 3. Economic parameters used to calculate NPV for the base case model (the values of those parameters are

extracted from reference [44])

Item	Value	Unit
Royalty	17%	-
Federal income tax	35%	-
Oil price, r_o	50	\$/bbl
Water injection cost, $r_{w,inj}$	1.03	\$/stb
Produced water treatment cost, $r_{w,pro}$	0.64	\$/stb
CO_2 injection cost, r_{co2}	0.85	\$/MSCF
CO_2 purchase price, $r_{co2,p}$	1.72	\$/MSCF
CO_2 storage credit, $q_{co2,store}$	45	\$/ metric ton
Inflation rate, r_b	5%	-
Capital expenditure, $CAPEX$	10 MM	\$

Figure 1 shows the results of the base case model.

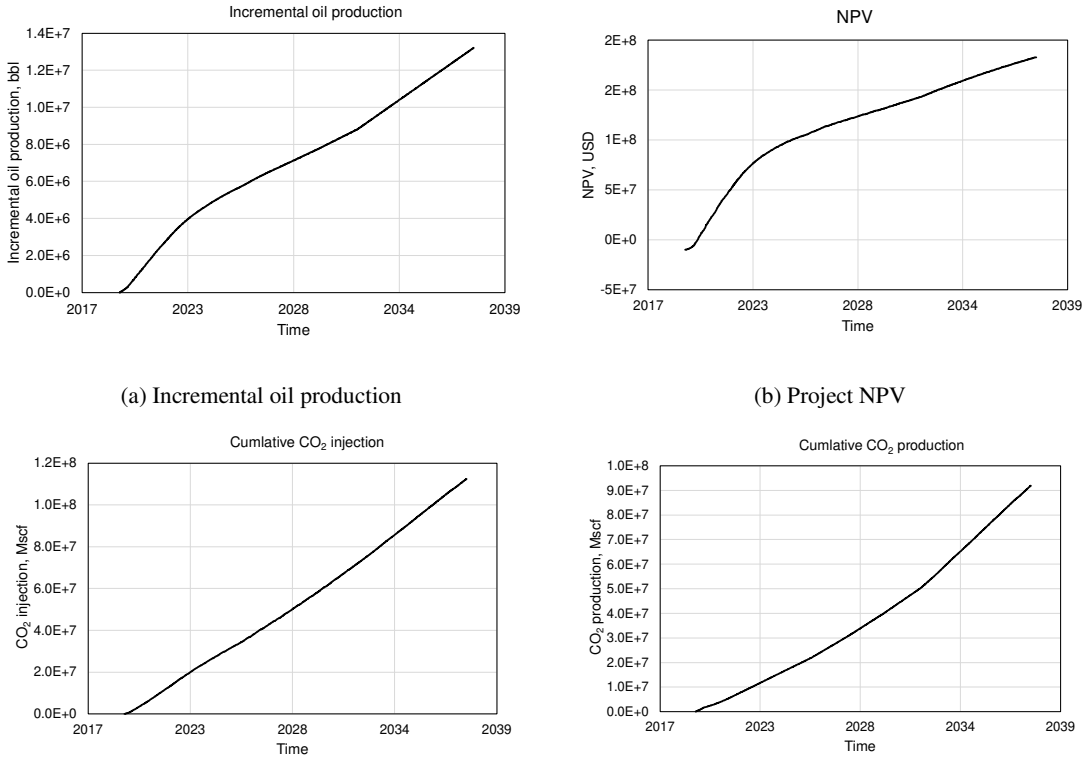

(a) Incremental oil production

(b) Project NPV

(c) Cumulative CO_2 injection

(d) Cumulative CO_2 production

Figure 1. Simulation results of the base case model.

Some crucial results of the base case model are summarized in Table 4:

Table 4. Results of the base case model

Item	Unit	Value
Incremental oil production	MM bbl	13.2
Incremental CO_2 storage volume	MM metric ton	1.06
Project NPV	USD	1.83×10^8
Cumulative Oil Production by Aug 2019	MM bbl	3.63
Cumulative Oil Production by Jan 2038	MM bbl	16.8
Cumulative CO_2 storage by Jan 2038	MM metric ton	2.36
% Storage of purchased CO_2	percentage	81.19%

It is observed that, in the base case model, the cumulative oil production at the end of the prediction time is 16.8 MM bbl; and the total CO_2 storage during the 20-years prediction is 2.36 MM metric tons, which takes up approximately 81.2% of the total purchased CO_2 according to the predefined CO_2 purchase plan. The project NPV is predicted to be 1.83×10^8 U.S. dollars. In the work described in the next section, by using the developed machine-learning-based optimization workflow, the three considered objectives are improved over the base case. For the convenience of discussion, the objective functions are defined as:

f_1= cumulative oil production by Jan. 2038

f_2 = cumulative CO_2 storage by Jan. 2038

f_3 = project NPV

4. SVR Assisted Multi-Objective Optimization Workflow

4.1 Sensitivity analysis

A sensitivity analysis study was performed to investigate the impact of operational parameters on the objective functions. Those with a high impact on oil production and CO_2 storage were selected

and utilized in the following optimization work. The selection of parameters used in the sensitivity analysis targets those that could be operated by the field engineers. A total of 37 operational parameters were used to conduct sensitivity analysis. As shown in Table 5, 12 parameters were selected due to their high impact on either oil production or CO_2 storage amount.

Table 5. Summary of selected parameters used in optimization work

Rank	Operational parameter	Unit	Base value	Min	Max
1	Field oil production rate from PD1 to PD4	STB/day	3500	2500	4500
2	Field oil production rate for PD8	STB/day	2000	1500	3500
3	Gas cycle for WAG B1 group in PD2	month	3	2	12
4	Water cycle for WAG B1 group in PD2	month	1	0	3
5	Gas cycle for WAG D1 group in PD4	month	3	2	12
6	Gas cycle for WAG D2 group in PD4	month	7	2	12
7	Gas cycle for WAG D3 group in PD4	month	9	2	12
8	Gas cycle for WAG D4 group in PD4	month	1	2	12
9	Water cycle for WAG D1 group in PD4	month	1	0	3
10	Water cycle for WAG D2 group in PD4	month	1	0	3
11	Water cycle for WAG D3 group in PD4	month	1	0	3
12	Water cycle for WAG D4 group in PD4	month	1	0	3

During the development of the CO2-WAG project, some producers or nonuse wells will be converted into WAG wells according to previous studies and field operator's suggestions [28]. Those new-proposed WAG injectors will be queued to come on stream based on CO2 availability and/or project anticipated schedule. The WAG wells are divided into various groups for more flexible controls and the wells in the same group will have the same operational parameters. The alphabets in the name of the operational parameters represent different groups of the WAG wells and those numbers meaning different time periods.

4.2 Preparation of initial training dataset

The proxy model is trained using synthetic data generated from high-fidelity numerical simulation models. Therefore, a certain volume of batch simulation realizations is sent to prepare the knowledgebase to develop the Gaussian-SVR proxy models. Figure 2 displays the structure of the dataset used in this part of the work. Here each set of training data contains 12 input parameters listed in Table 5. The training outputs (targets) include cumulative oil production, cumulative CO_2 storage amount, and project NPV.

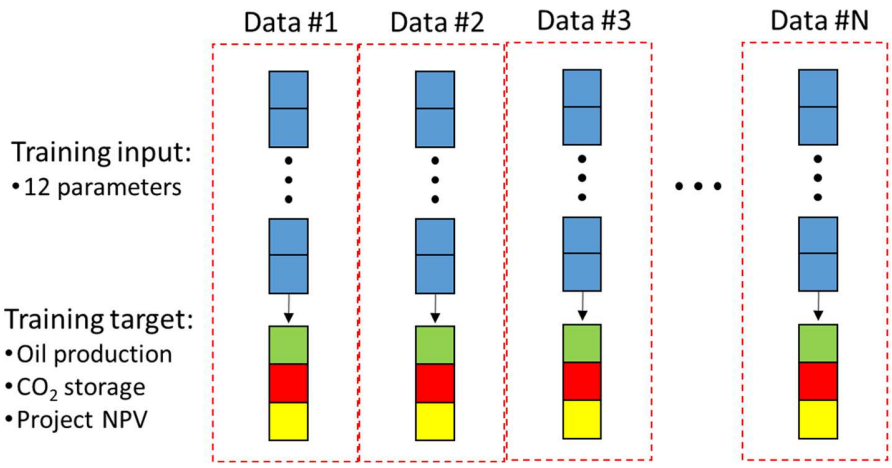

Figure 2. Structure of training dataset. The training targets include cumulative oil production (green square), CO_2 storage amount (red square) and project NPV (yellow square) at the end of the forecasting period. Training inputs are 12 parameters represented by blue squares.

4.3 Proxy modeling using Gaussian-SVR

Supported vector regression with Gaussian kernel is a robust method for solving linear and nonlinear regression problems[45]. In Gaussian-SVR, the use of the Gaussian kernel will convert a nonlinear problem to linear regression by mapping the original input space into a higher dimensional feature space where the problem could be solved linearly. The process of using

Gaussian-SVR to solve nonlinear regression problems can be expressed as Eq. 2 and Eq. 3, with the Gaussian kernel function expressed as Eq. 4.

$$L(\alpha,\alpha^*) = \text{maximize} \begin{cases} -\frac{1}{2}\sum_{i,j=1}^{l}(\alpha_i-\alpha_i^*)(\alpha_j-\alpha_j^*)K(x_1,x_2) \\ -\varepsilon\sum_{i=1}^{l}(\alpha_i+\alpha_i^*)(\alpha_j-\alpha_j^*)+\sum_{i=1}^{l}y_i(\alpha_i-\alpha_i^*) \end{cases} \quad \text{(Eq. 2)}$$

$$\text{subject to } \sum_{i=1}^{l}(\alpha_i-\alpha_i^*)=0 \text{ and } \alpha_i,\alpha_i^* \in [0,C] \quad \text{(Eq. 3)}$$

$$K(x_i,x_j) = \exp\left(-\frac{\|x_i-x_j\|^2}{2\sigma^2}\right) \quad \text{(Eq. 4)}$$

The setting-up of the Gaussian-SVR model will determine the prediction performance of the trained proxy model. Parameters need to be carefully designed to obtain good proxy models. The hyperparameters to be optimized in proxy modeling work are summarized in Table 6:

Table 6. Hyperparameters used in the proxy modeling

Hyperparameters	Symbol	Function
Constant	C	Control the penalty implemented on those inputted data that violate the margin.
Half-width of the insensitivity zone	ε	Determine the zone where observations are not considered as supported vectors in the SVR model
Kernel scale factor	$\frac{1}{2\sigma^2}$	Determine how the kernel captures the local similarity

The Bayesian optimization algorithm (BOA) is an efficient method for the optimization of hyperparameters when computational power is limited. One very important feature differentiating BOA from other optimization algorithms is that BOA will use all available information based on the previous estimation of the objective function rather than simply relying on a local gradient and Hessian approximation,[46, 47] which means this method can provide a higher possibility to find the optimal solution in limited search works.

The application of BOA builds on two main steps.[46] Firstly, one should select a prior over function that will express assumptions about the function being optimized. Secondly, an acquisition function from the model posterior is used to determine the next point.

For the first step, one commonly used method is Gaussian Processes (G.P.) due to its flexibility and tractability.[46]

The calculation of the acquisition function (or utility function) is based on the predictive mean function $\mu(x;\{x_n,y_n\},\theta)$ and the predictive variance function $\sigma^2(x;\{x_n,y_n\},\theta)$.

The mean function and covariance are combined in the acquisition function in a certain way, and the acquisition function will be used to determine those new sampling data that are most likely to be the best ones. Commonly used acquisition functions include the Probability of Improvement, Expected Improvement, and G.P. Upper Confidence Bound.[46] In the training work, the knowledge base is used to train the proxy model using the K-fold cross-validation algorithm (Figure 3). In K-fold cross-validation, the original training database will be equally split into K groups. When training the proxy model, one group of data will be used as blind test data, while the other $K-1$ group will be used as the training database. Thus, a proxy model with a certain combination of hyperparameters will be trained K times using the K-fold cross-validation algorithm.

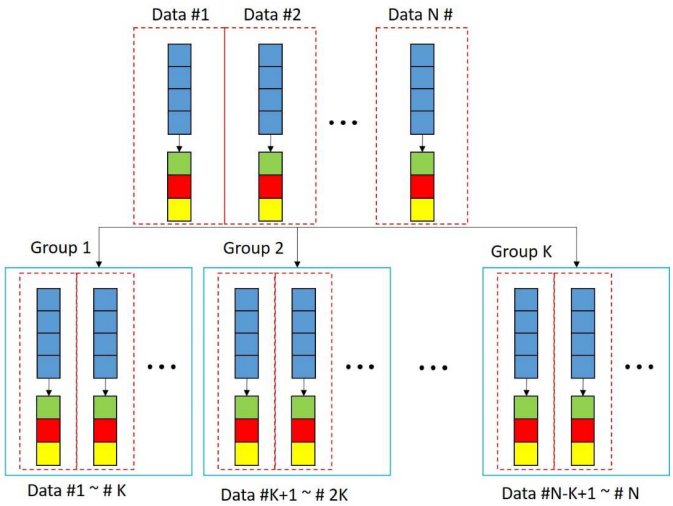

Figure 3. Schematic plot of K-fold cross-validation. In K-fold cross-validation, the original training database (containing N sets of sample data) will be equally divided into K groups. When training a proxy model, K-1 groups of data will be used as training data and the left group's data will be used to blind test the trained proxy. The process will be looped K times until every group of data has been used in blind tests.

After the trained proxy model is obtained, the absolute relative error (E) between proxy prediction and simulation targets is calculated based on Eq. 5:

$$E = \frac{1}{m}\sum_{n=1}^{m}\frac{|T_n - Y_n|}{T_n} \quad \text{(Eq. 5)}$$

where T_n is the observed target value of n-th output, Y_n is the predicted value of n-th output, and m is the number of outputs (training targets).

The main advantage of the K-fold cross-validation method is that it will not waste the data obtained already. This can be very important when obtaining more data is difficult (i.e., when conducting more numerical simulations will take a very long time). However, this approach can lead to extra computational time when using it in a training proxy model. That is why in this work, Bayesian optimization is chosen as the hyperparameters optimization method.

4.4 Structuring the SVR Assisted Multi-Objective Optimization Workflow

As shown in Figure 4, the development of SVR proxy enables the structuring of the multi-objective optimization workflow by coupling it with the MOPSO algorithm. Pareto optimal solutions are generated to include various CO_2-WAG injection designs. Although the SVR proxy is well trained with an error margin of less than 2%, inevitable uncertainties could be introduced to the Pareto fronts. An iterative loop is added to the workflow which validates the solution with the high-fidelity numerical simulator. When large disparities are observed, new data samples will be added to retrain the SVR proxy until a prescribed tolerance is reached. In the following discussions, the robustness of the proposed workflow will be validated by optimizing the CO_2-WAG injection project of the FWU field.

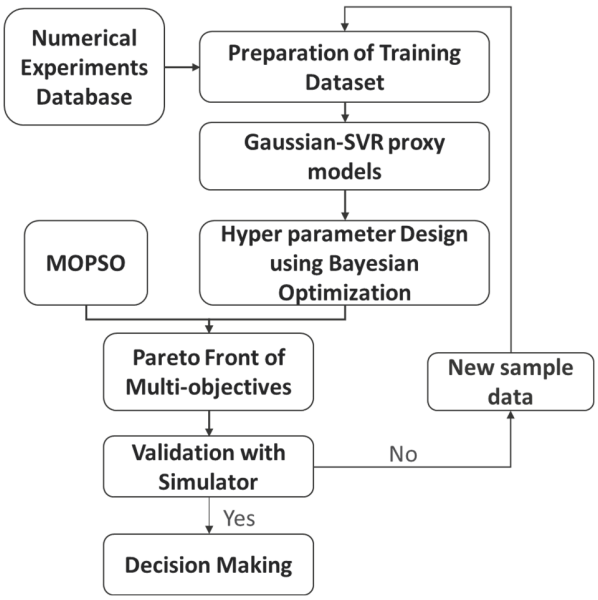

Figure 4. Schematic chart of procedures of the workflow.

5. Results and Discussion

5.1 Optimization using Developed Multi-Objective Optimization Workflow

The proposed workflow is employed to optimize the CO_2-WAG operational parameter of the FWU field case. As shown in Table 7, the initial trial of the optimization indicates that the disparity between the Pareto fronts generated by the proxy and numerical simulator become less than 5% after three sets of new data samples are added.

Table 7. Summary of sample datasets used in each iteration

Number of iterations	Sample datasets used	Error
1	140	25.8%
2	39	20.5%
3	38	3.8%
Total	217	-

Figure 5 displays the Pareto fronts generated after each iteration when two objectives are considered (incremental oil production and incremental CO_2 storage). Notably, the incremental oil production and incremental CO_2 storage volume exclude the contribution of the history matching period (2011 to 2019).

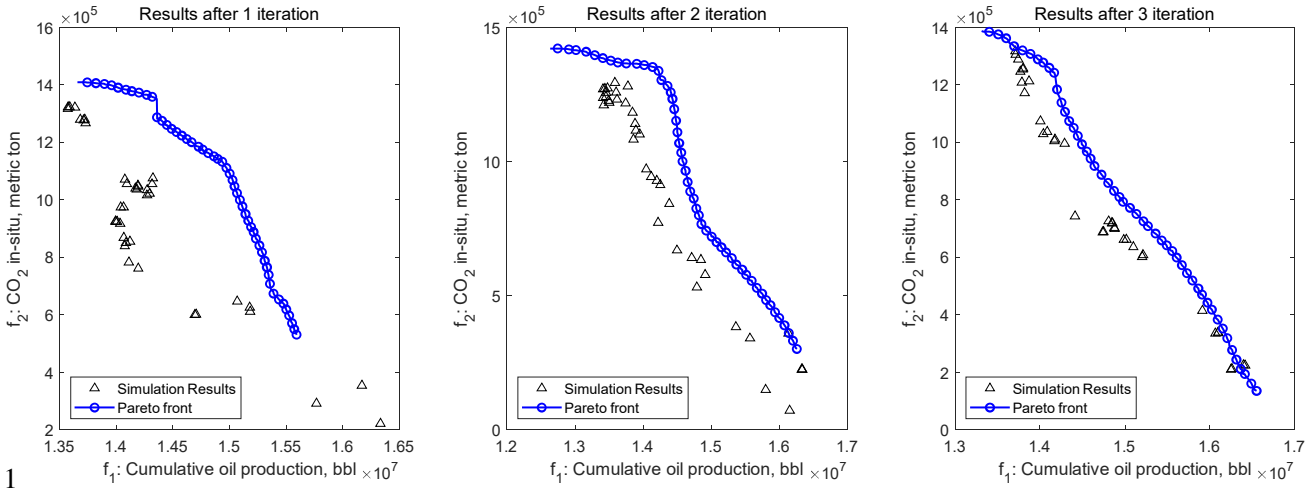

Figure 5. Pareto front (incremental oil production and incremental CO_2 storage) generated in each iteration, the difference between prediction using proxy and simulation results is 3.8% after three iterations.

The Pareto fronts indicate that the incremental oil production of the solutions on the Pareto front ranges from 13.5 MM bbl to 16.5 MM bbl, and the incremental CO_2 storage ranges from 0.1 to 1.4 MM metric tons. The project NPV can also be considered in the optimization study to structure a Pareto front in three-dimensional objective function space as shown in Figure 6.

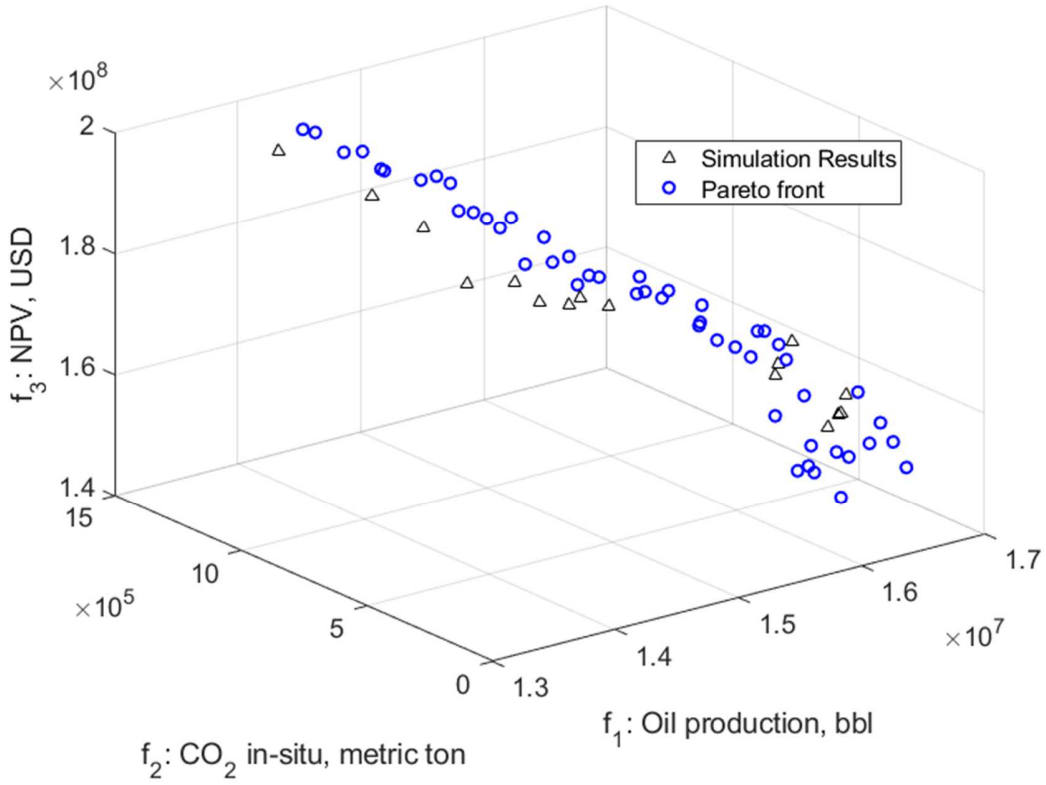

Figure 6. Pareto front (incremental oil production, incremental CO_2 storage and project NPV).

To further investigate the Pareto front, its projection views into the 2-D planes are displayed in Figure 7. The projection view into f_1-f_2 plane (Figure 7a) exhibits good agreement with the two-dimensional Pareto front, which confirms the stability of the Pareto optimal solution generated by the proposed workflow. The range of the incremental oil production is from 13.8 MM bbl to 16.8 MM bbl, and the incremental CO_2 storage ranges from 0.17 to 1.38 MM metric tons, which are also consistent with the observed in the Pareto optimal solution of two objectives. The range of the final project NPV is from about 1.45×10^8 to 2.0×10^8 U.S. dollars.

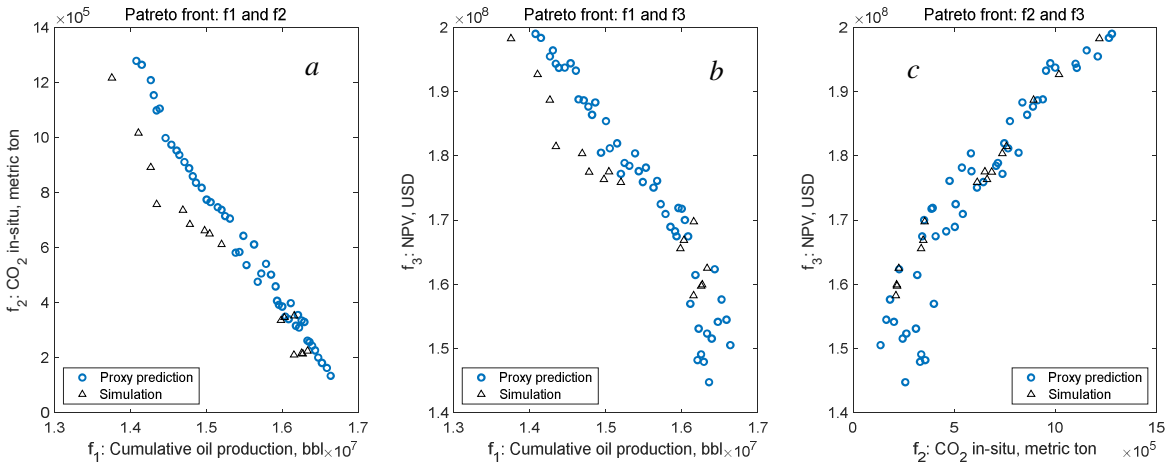

Figure 7. View the Pareto front considering 3 objectives in a 2-D plot. (a) plot from f_1 (incremental oil production) and f_2 (incremental CO_2 storage volume) plane; (b) the plot from f_1 (incremental oil production) and f_3 (project NPV) plane; and (c) the plot from f_2 (incremental CO_2 storage volume) and f_2 (project NPV) plot.

Practical CO_2-WAG operations would demand to sustain the reservoir pressure above the minimum miscible pressure (MMP) and ensure a miscible displacing front.[48] Laboratory experiments suggest that the minimal miscible pressure (MMP) of the hydrocarbon fluid in Morrow B sandstone with CO_2 is approximately 4000 psi.[28] To make sure average reservoir pressure is maintained above the MMP, a proxy model is developed to predict the average reservoir pressure and constrain the multi-objective optimization process.[19] The constrained Pareto fronts are shown in Figure 8.

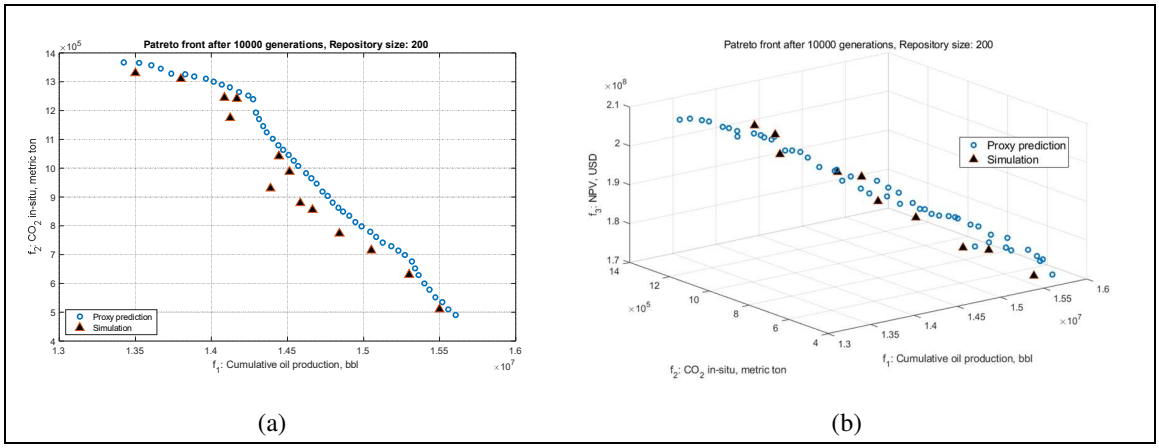

(a) (b)

Figure 8. Comparison between the Pareto front and numerical simulation results using some of the optimized input parameters: (a) 2-objectives and (b) 3-objectives.

Compared with the Pareto fronts generated without average reservoir pressure constraints, the range of objectives covered by those with constraints is narrowed. Table 8 summarizes the comparison between the ranges covered by Pareto fronts with and without the pressure constraint. In the CO_2-WAG project ongoing in the Farnsworth unit, CO_2 storage and oil production are conflicting objectives, increasing in CO_2 storage will typically lead to a reduction in oil production. This is because increasing CO_2 storage volume needs injecting more CO_2, which leads to the reduction in water injections to displace additional oil to be produced. The results indicate that after the pressure constraints are imposed, the lower limit of the CO_2 storage volume range increased while the upper limit of incremental oil production range was reduced. This indicates that those solutions with low CO_2 volume storage and high oil productions are removed from the Pareto fronts. When oil production is high (for those Pareto optimal solutions, CO_2 storage volume is low at the same time), the reservoir depletes quickly and so does the reservoir pressure. At the same time, more oil production at the latter stage of the project would lead to more CO_2 production and lower

the CO_2 storage volume.

Table 9 summarizes the comparison between the results of the base case and the results of solutions on the Pareto front. It shows that the project response suggested by the Pareto optimal outperforms the base case result. More importantly, the developed Pareto front provides not just one solution, but a set of optimized solutions so that decision-makers can select solutions from the repository to meet specific requirements. For example, if the project required that 90% of CO_2 should be stored, then the decision-maker could filter out those solutions with a CO_2 storage percentage higher than 90% and find which one has the highest oil production or project NPV from the rest of the solutions.

Table 8. Comparison between the Pareto fronts with/without average reservoir pressure constraint

		With constraint	Without constraint
2-objectives	Oil	13.7~15.6 MM bbl	13.4~ 16.5 MM bbl
	CO_2	0.49~1.39 MM metric ton	0.18~1.40 MM metric ton
3-objectives	Oil	13.3~15.7 MM bbl	14.0~ 16.8 MM bbl
	CO_2	0.42~1.4 MM metric ton	0.18~1.4 MM metric ton
	NPV	1.70×10^8~2.05×10^8 USD	1.42×10^8~2×10^8 USD

Table 9. Comparison between the results of the base case and optimized solutions

Item	Unit	Value
Base Case Results		
Incremental oil production	MM bbl	13.2
Incremental CO_2 storage volume	MM metric ton	1.06
Project NPV	MM USD	183
Cumulative Oil Production by Jan 2038	MM bbl	16.8
Cumulative CO_2 storage by Jan 2038	MM bbl	2.36
% Storage of purchased CO_2	percentage	81.19%
Optimized Solutions Results		
Range of incremental oil production	MM bbl	13.3~15.7
Range of incremental CO_2 storage volume	MM metric ton	0.42~1.4

Range of project NPV	MM USD	170~205
Max cumulative oil production	MM bbl	19.3
Max cumulative CO_2 storage	MM metric ton	2.7
Max project NPV	MM USD	205
Max % Storage of purchased CO_2	percentage	92.9%

1

2 ***5.2 Optimization Results under Uncertainty***

3 In the optimization under uncertainty, the true objective function value is unknown, so some
4 approaches should be used to estimate the confidence of the optimized results. In this work, the
5 uncertainty of the optimization results is considered by using a combined objective function with
6 the risk aversion factor introduced by Couet et al.[49] This approach is expressed as Eq. 6:

7 $$\text{Combined objective function } (\text{C.F.}) = \mu - \lambda \times \sigma \qquad \text{(Eq. 6)}$$

8 where μ is the mean, λ is the risk aversion factor, and σ is the standard deviation.

9 The risk aversion factor λ represents different levels of confidence in the results. For instance,
10 when λ equals 0 it means there is a 50% probability that the true objective function value is greater
11 than the computed objective function, while when λ equals 2 it means there is a 98% possibility
12 the true objective function value is larger than the computed objective function. Figure 9 displays
13 the results of optimization under uncertainty when two objectives and three objectives are
14 considered, respectively.

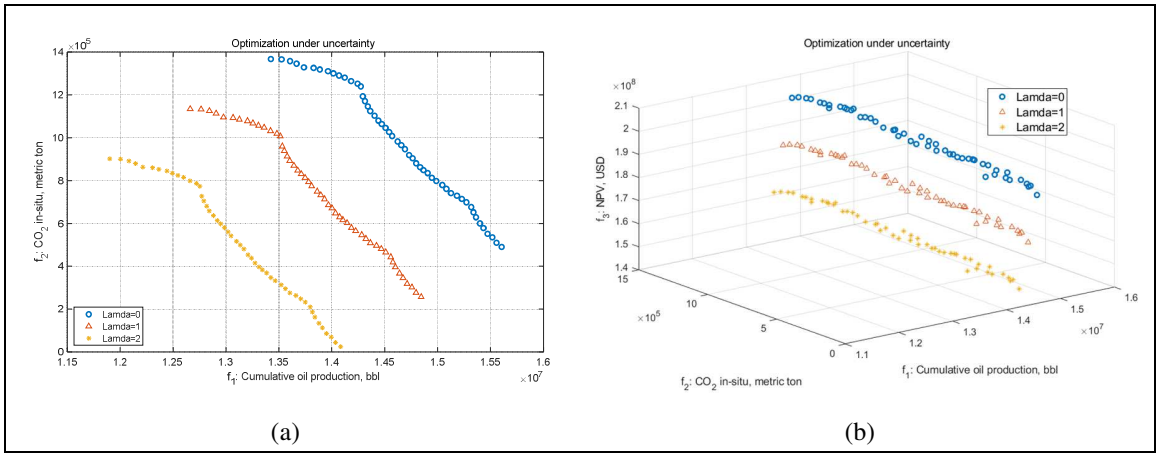

(a) (b)

Figure 9. Comparison among the Pareto fronts with different risk factors: (a) 2-objectives and (b) 3-objectives.

Table 10 summarizes the maximal incremental oil production, maximal incremental CO_2 storage volume, and maximal project NPV at the end of prediction time. As the λ increases, the maximum the Pareto fronts shift towards the lower ends of the objective function domains, which indicate more conservative techno-economic project assessments.

Table 10 The maximal value of each objective at the end of forecasting time

Risk aversion factor	Oil production, MM bbl	CO_2 storage, MM metric ton	NPV, MM $
$\lambda = 0$	15.8	1.37	205.60
$\lambda = 1$	15.0	1.13	193.56
$\lambda = 2$	14.2	0.90	182.27

5.3 The Effect of Oil Price on Optimization Results

Considering the drastic vibrations of the crude oil market, it is necessary to investigate the impact of oil price on the optimization results. Assuming a base case oil price to be 50 USD/bbl, P10, P50 and P90 cases are investigated using oil prices of 70, 50 and 30 USD/bbl. P10 means that the true oil price has a 10% possibility to be higher than the presumed oil price, with P50 and P90 having a similar meaning. Except for oil price, other factors used in the NPV calculation are the same as the

values listed in Table 3. The three-objective Pareto fronts and the projection views are shown in Figure 10 and Figure 11, respectively.

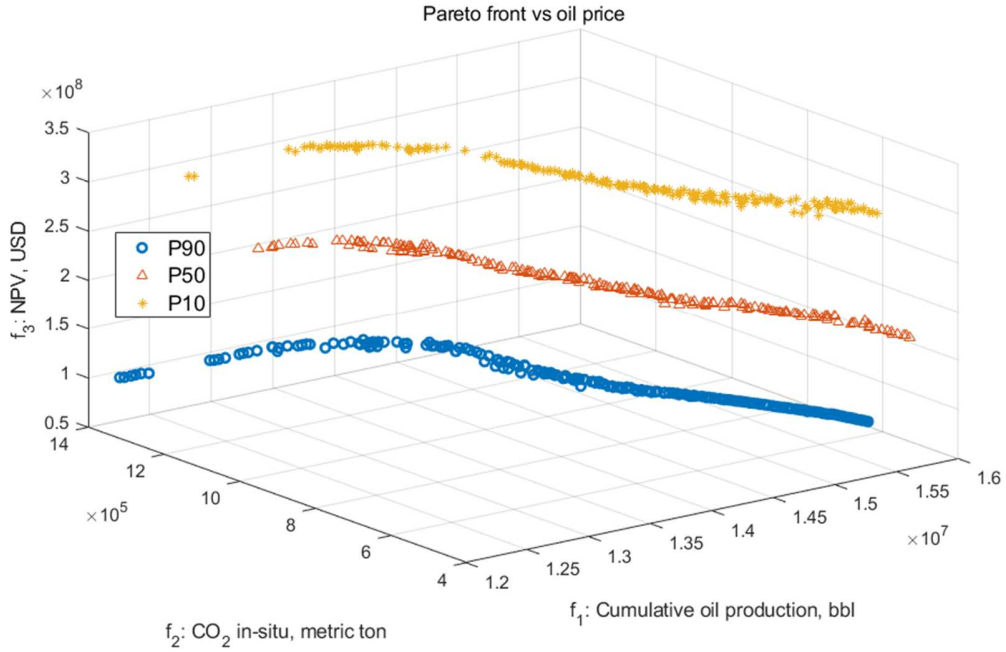

Figure 10. Comparison among the Pareto fronts with different oil prices.

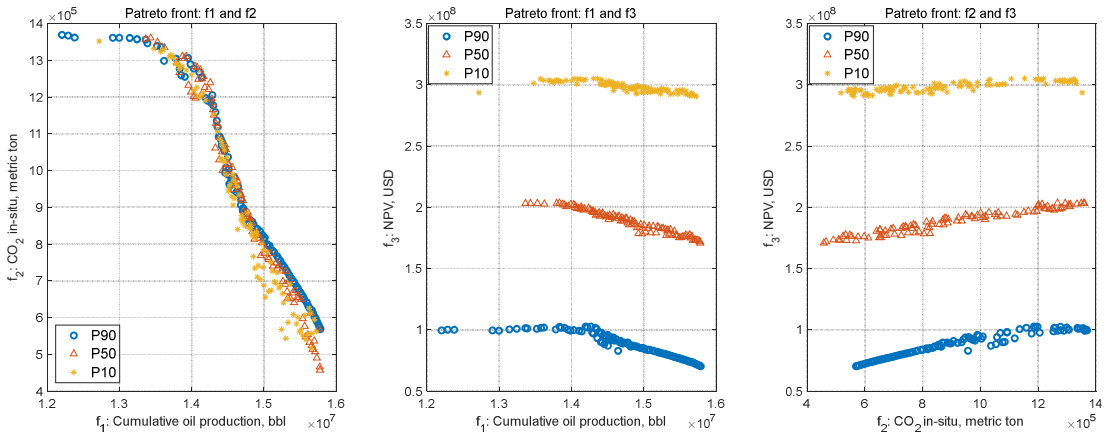

Figure 11. A 2-D view of the comparison among the Pareto fronts with different oil prices.

To validate the optimization results obtained, for each of the generated Pareto fronts, some

solutions located on the Pareto front are selected and their optimized input parameters are revisited by the original numerical simulation model. The simulation results are compared with their corresponding Pareto fronts that are generated using proxy models.

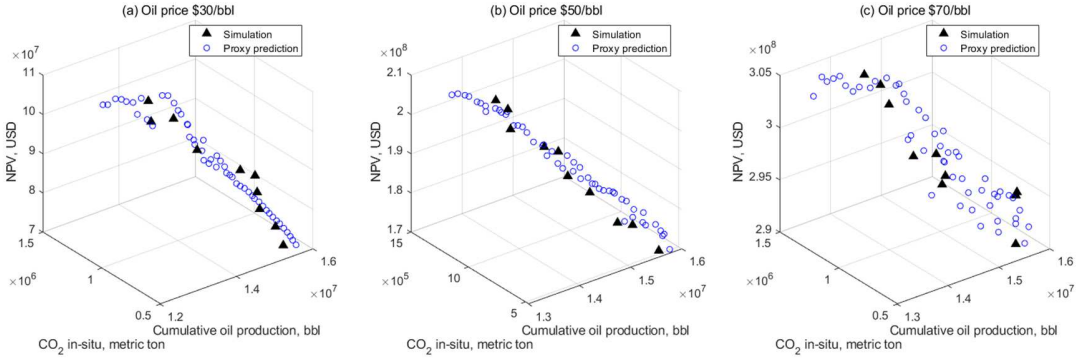

Figure 12. Comparison between proxy predictions and simulation results: Proxy predictions (circle) and simulation results (black triangle). CO_2 storage credit: \$45/ metric ton.

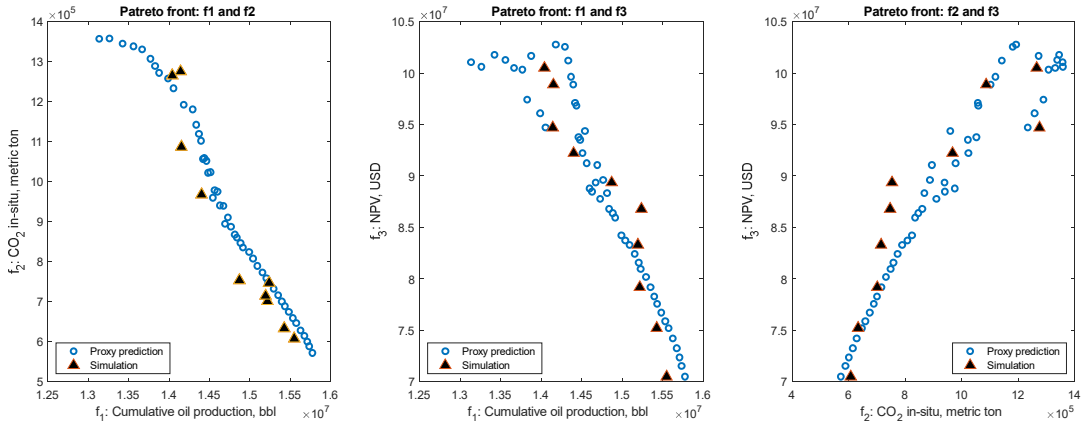

(a) CO_2 credit: \$45/ metric ton of CO_2 storage, oil price: \$30/bbl.

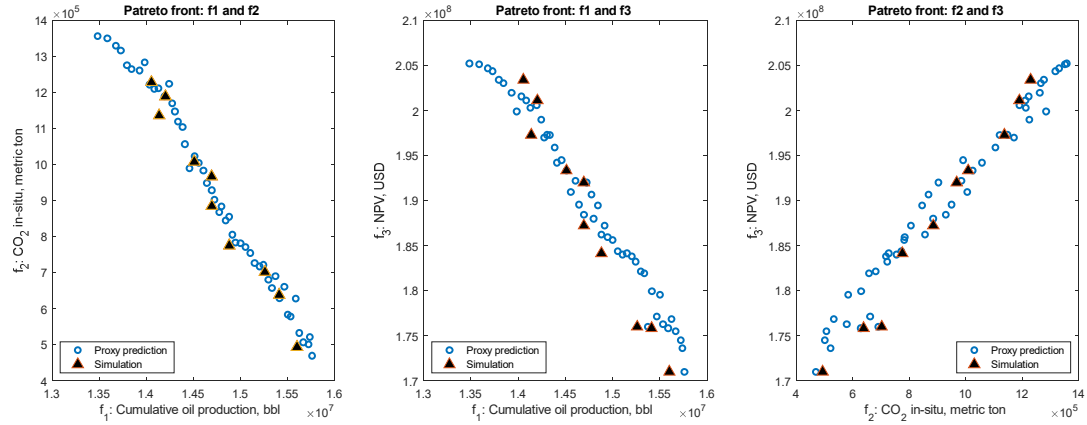

(b) CO_2 credit: \$45/ metric ton of CO_2 storage, oil price: \$50/bbl.

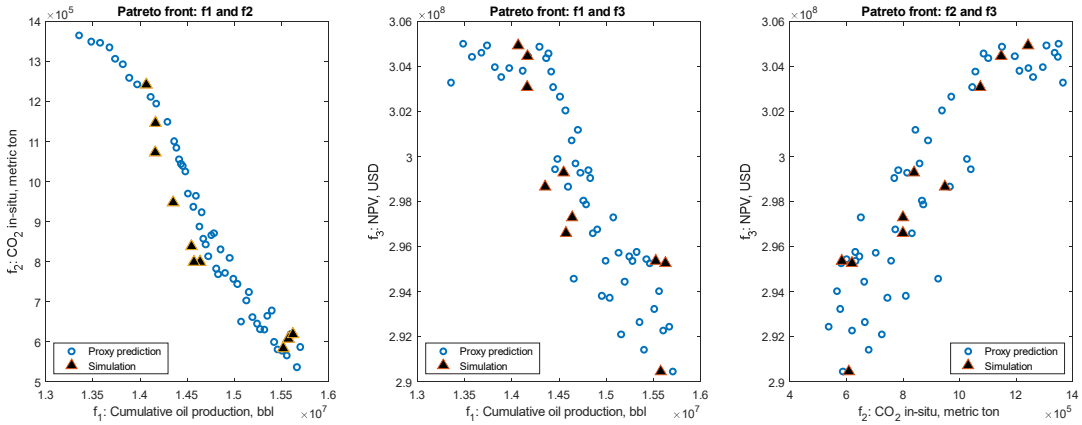

(c) CO_2 credit: \$45/ metric ton of CO_2 storage, oil price: \$70/bbl.

Figure 13. A 2-D view of the comparison between Pareto fronts generated using different oil prices (P90, P50 and P10) and corresponding simulation results (CO_2 credit: \$45/ metric ton).

Figure 12 and Figure 13 confirm the validity of these generated Pareto fronts by comparing the

results with the high-fidelity numerical simulator. It is observed that the shape of the generated Pareto front in the f_1-f_2 plane is very similar for all three levels of oil price, meaning that the change of the oil price has a negligible impact on the shape of the Pareto front in oil production and CO_2 storage volume domain. This indicates that when only oil production and CO_2 storage volume are considered as objectives, the Pareto-optimal solutions are mainly determined by operational development strategies, but not those economic factors to calculate project NPV. Nevertheless, the oil price has a great influence on project NPV. When oil prices change from \$30/bbl to \$70/bbl, it is obvious that both the higher and lower limit of the project NPV of the Pareto-optimal solutions are increased.

More importantly, when investigating Pareto front from $f_1 – f_3$ plane and $f_2 – f_3$ plane, it was found that the highest NPV is not always achieved at either the highest oil production or the highest CO_2 storage. This is because the NPV calculation considers many economic terms such as water injection cost, produced water treatment cost, CO_2 injection cost, and CO_2 purchase cost. The increase in oil production can lead to more benefits directly from selling oil, but it also increases the water injection and production as the byproduct, as well as increasing produced CO_2 so that the cost for those parts will increase and hence reducing the final project NPV. For the CO_2 storage, the reason is similar. Increasing CO_2 storage volume will reduce the production of oil and increase the costs of CO_2 injection and will lead to more cost on CO_2 purchases at the same time. The consideration of different economic factors in project NPV calculation makes the optimization results considering oil production, CO_2 storage, and project NPV very complex and even

counterintuitive. The trade-offs among those three objectives are much more difficult to evaluate using traditional methods.

Thus, when considering the project NPV as a third optimization objective, the Pareto-front-based multi-objective optimization methodology helps evaluate this kind of trade-off and hence providing more information and flexibility to the decision-maker.

5.4 The effect of a CO_2 storage credit on optimization results

This work will also evaluate the impact of CO_2 storage credit on the optimization results. Aside from the oil price, another significant economic factor to determine the economic outcomes of a CCUS project is the consideration of any tax credit for CO_2 storage. In the U.S., according to related policies (such as Section 45Q of the US tax code [50]), the government will provide incentives to qualified carbon storage projects to encourage more anthropogenic CO_2 to be sequestered underground. The Section 45Q tax credit for carbon capture projects provides a foundational policy for increasing the deployment of carbon capture projects in the U.S. It states that the tax credit amount can be from \$35/ metric ton to \$50/ metric ton of CO_2 storage depending on different project types. In the previous section, the CO_2 credit is presumed to be \$45/ metric ton of CO_2 storage. In the following work, the CO_2 credit is set to be \$35/ metric ton of CO_2 storage and the multi-objective optimization is redone once to compare how the CO_2 storage credit influences the optimization results. The optimization process is performed under the condition that CO_2 tax credits are set to be \$35/ metric ton of CO_2 storage and the oil price is presumed to be at three different possibility levels (e.g. \$30, \$50, \$70), while the other economic parameters remain the

same as what is listed in Table 3.

Figure 14 and Figure 15 show the generated Pareto fronts for different oil prices. Some solutions located on the Pareto front are selected and their optimized input parameters are revisited by the original numerical simulation model to validate the optimization results obtained. Results of the comparison are also displayed in Figure 14 and Figure 15.

Figure 16 compares the Pareto fronts generated using two different CO_2 credits in 2-D planes. It was found that, for different values of CO_2 credit used, the shape of the generated Pareto front in the f_1- f_2 plane stays almost the same. This tells us that once again, the upper and lower limits of the incremental oil production and incremental CO_2 storage volume of the Pareto front are mostly determined by the petrophysical properties of the numerical model. Changing economic factors will not lead to a significant impact on the range of incremental oil production and incremental CO_2 storage volume covered by the developed Pareto front.

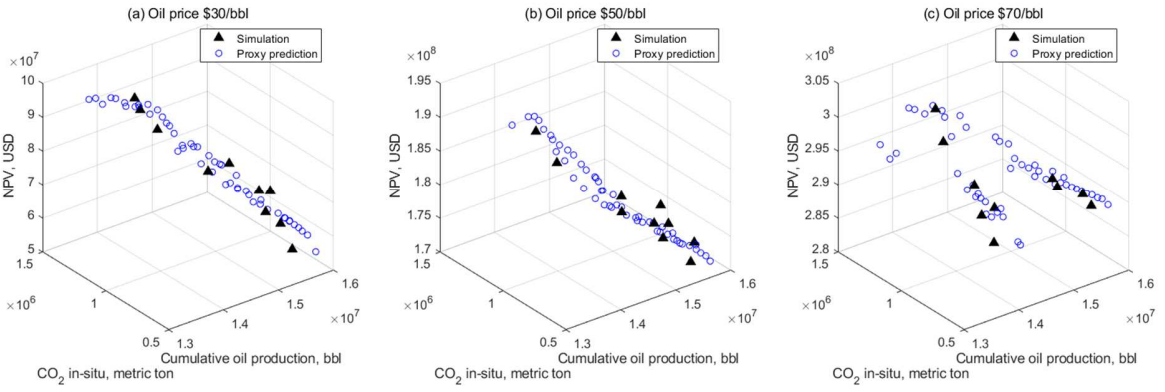

Figure 14. Comparison between proxy predictions and simulation results: Proxy predictions (circle) and simulation results (black triangle). CO_2 storage credit: $35/ metric ton.

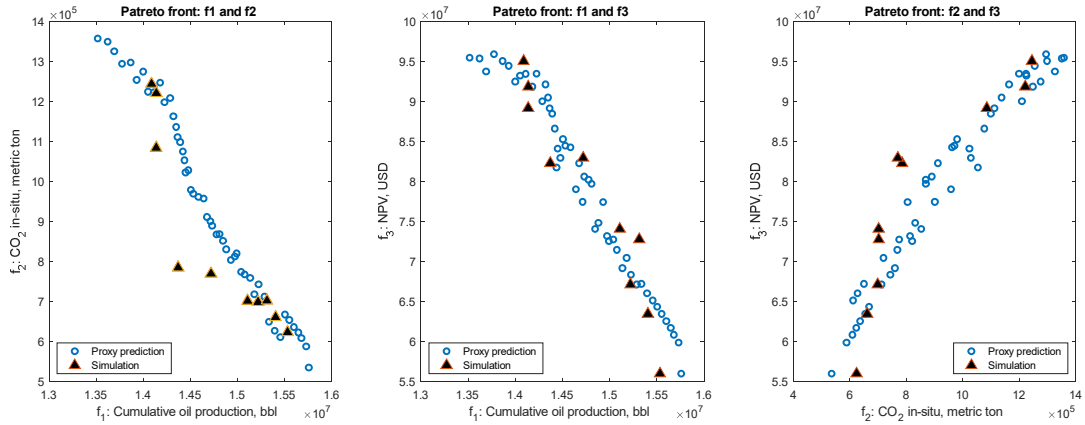

(a) CO_2 credit: \$35/ metric ton of CO_2 storage, oil price: \$30/bbl.

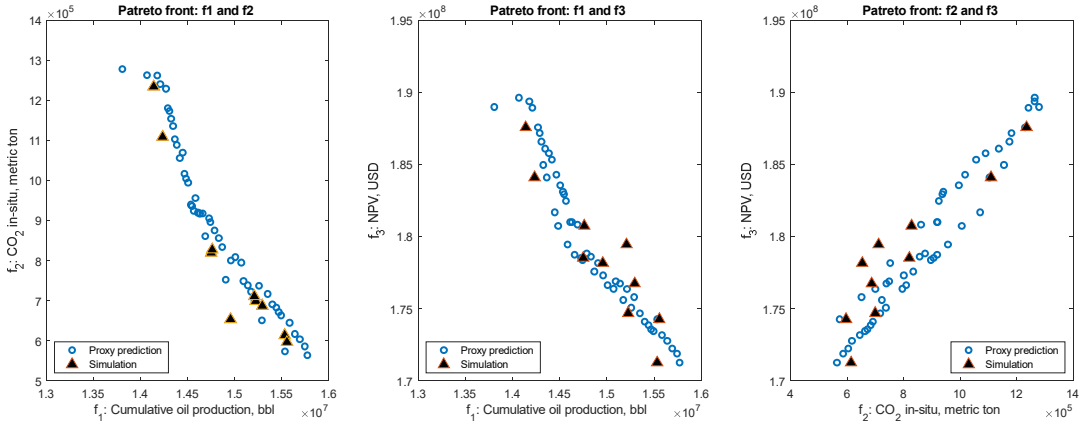

(b) CO_2 credit: \$35/ metric ton of CO_2 storage, oil price: \$50/bbl.

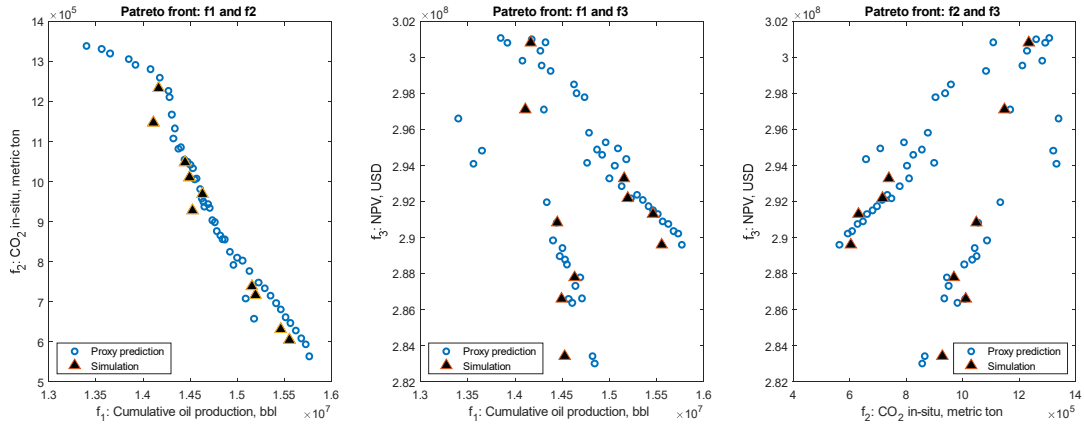

(c) CO_2 credit: \$35/ metric ton of CO_2 storage, oil price: \$70/bbl.

Figure 15. A 2-D view of the comparison between Pareto fronts generated using different oil prices (P90, P50 and P10) and corresponding simulation results (CO_2 credit: \$35/ metric ton).

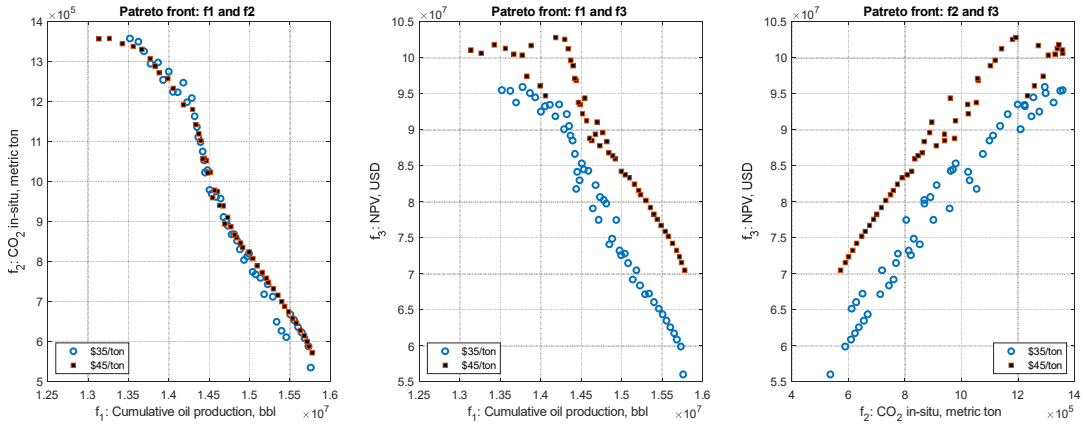

(a) Oil price: $30/bbl.

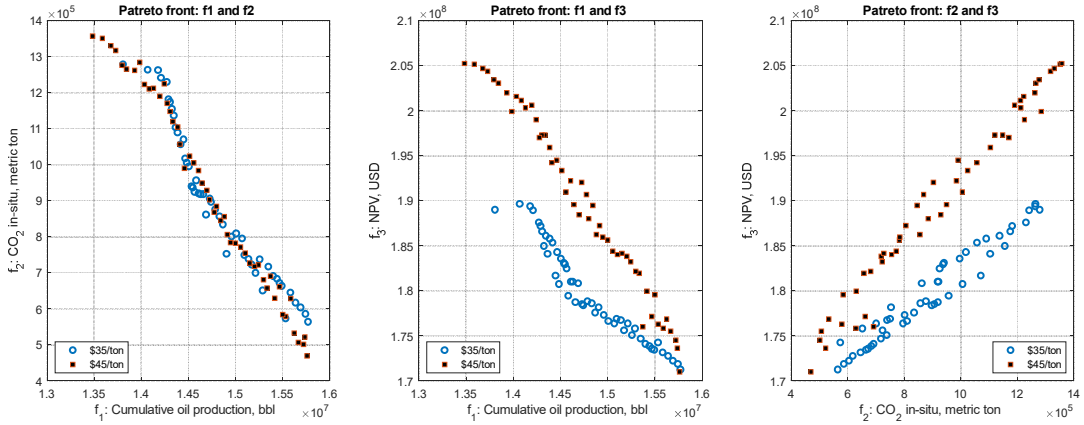

(b) Oil price: $50/bbl.

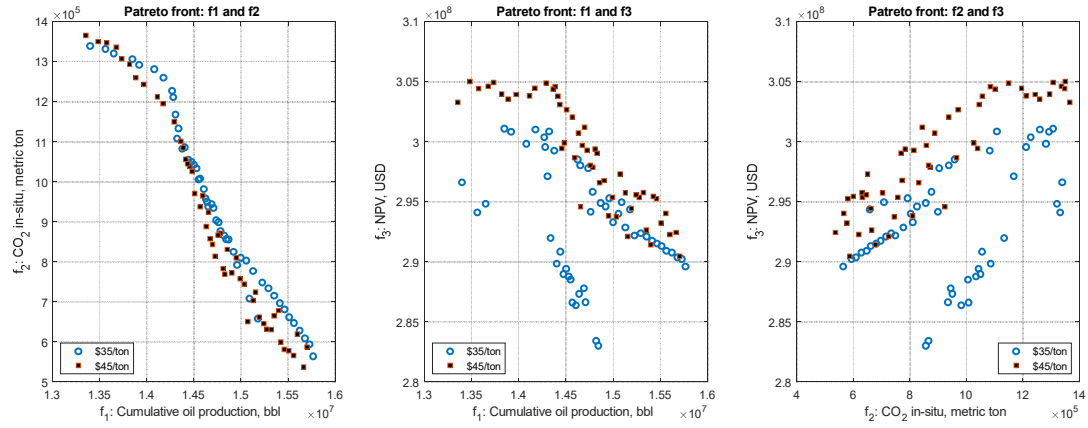

(c) Oil price: $70/bbl.

Figure 16. A 2-D view of the comparison between Pareto fronts under different CO_2 storage credits: $35/ metric ton (circle) and $45/ metric ton (square).

However, when CO_2 credit is increased, the upper and lower limits of the project NPV are increased since more profit can be obtained when the same volume of CO_2 is sequestered underground. The shapes of developed Pareto fronts in the f_1- f_3 plane and f_2- f_3 plane become very different when compared against those using \$45/ metric ton of CO_2 credit. The trend of project NPV is not monotonous, but demonstrates irregularity.

6. Conclusion and Summary

In this work, a developed Pareto-front-theory-based multi-objective optimization workflow is applied to optimize the development strategies in cooperation with FWU's geological model. The development plan for a CO_2-WAG project is optimized according to a presumed CO_2 purchase plan of the following 20 years. Besides optimizing oil production and CO_2 storage, efforts are also given to assessing the project NPV that considers different economic parameters in its calculation. The impacts of oil price and CO_2 storage credit on project NPV are comprehensively studied. This research will serve as a benchmark and brings insights into the simultaneous optimization and techno-economic analysis of CCUS projects considering similar multiple objectives as the CO2-WAG project ongoing at FWU. The following conclusions are drawn from this work:

1. The developed Pareto-front-based multi-objective optimization workflow successfully structures the Pareto fronts considering two objectives and three objectives. The developed Pareto fronts are validated by comparing them with numerical simulation results using the same optimized input parameters.
2. When the average reservoir pressure is considered as an optimization constraint, the

corresponding Pareto fronts will be narrowed compared to those without such a constraint. The reason is that the optimization workflow will remove those solutions that will lead to great reservoir pressure depletion from the final generated Pareto front.

3. The formula used to calculate the project NPV makes the developed Pareto front considering NPV as the third objective very complex. It was found that the change in oil price and the CO_2 tax credit will significantly affect the generated Pareto front. However, the trade-offs among those three objectives are difficult to evaluate using traditional methods.
4. The Pareto-front-based multi-objective optimization methodology is very helpful in evaluating the trade-offs among those three objectives, and hence provides more information and flexibility to decision-makers.

Acknowledgment

Funding for this project is provided by the U.S. Department of Energy's (DOE) National Energy Technology Laboratory (NETL) through the Southwest Regional Partnership on Carbon Sequestration (SWP) under Award No. DE-FC26-05NT42591.

Appendix

Figure A- 1 shows the history matching results.

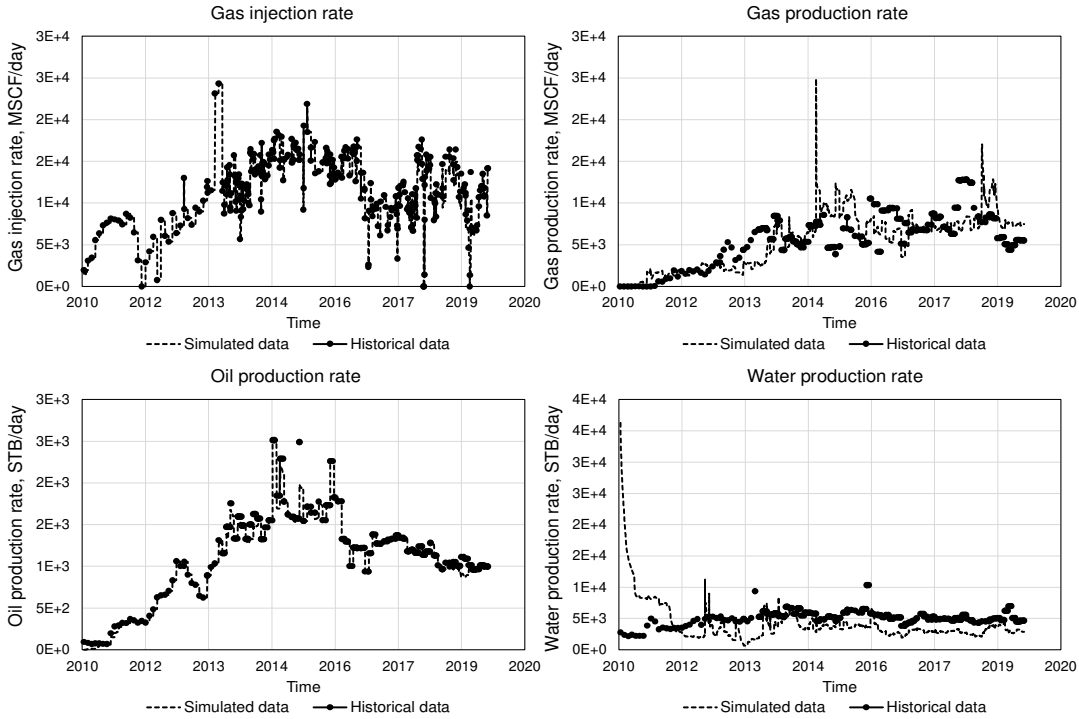

Figure A- 1 History matching results of the primary constraints imposed on the production (oil production rates), and the gas injection/production rates and water production rates

Table A - 1 summarizes the parameters used in the sensitivity analysis.

Table A - 1 Parameters used in the sensitivity analysis

Parameter name	Unit	Base value	Min	Max	Meaning
PD1_4FOPT	bbl/D	3500	2500	4500	Field oil production rate from PD1 to PD4
PD1_4PRBHP	psi	2000	1800	3500	Producer bottomhole pressure from PD1 to PD4
PD1_4WTR	stb/D	2500	2000	3000	Field water injection rate from PD1 to PD4
PD5_7FOT	bbl/D	3500	2500	4500	Field oil production rate from PD5 to PD7
PD8FOT	bbl/D	2000	1500	3500	Field oil production rate for PD8
PD1WA1GASCYC	month	3	2	12	Gas cycle for WAG A1 group in PD1
PD1WA2GASCYC	month	5	2	12	Gas cycle for WAG A2 group in PD1
PD1WA3GASCYC	month	7	2	12	Gas cycle for WAG A2 group in PD1
PD1WA4GASCYC	month	9	2	12	Gas cycle for WAG A2 group in PD1
PD1WA1WATCYC	month	1	0	3	Water cycle for WAG A1 group in PD1
PD1WA2WATCYC	month	1	0	3	Water cycle for WAG A2 group in PD1
PD1WA3WATCYC	month	1	0	3	Water cycle for WAG A3 group in PD1
PD1WA4WATCYC	month	1	0	3	Water cycle for WAG A4 group in PD1
PD2WA1GASCYC	month	3	2	12	Gas cycle for WAG B1 group in PD2

PD2WA2GASCYC	month	5	2	12	Gas cycle for WAG B2 group in PD2
PD2WA3GASCYC	month	7	2	12	Gas cycle for WAG B3 group in PD2
PD2WA4GASCYC	month	9	2	12	Gas cycle for WAG B4 group in PD2
PD2WA1WATCYC	month	1	0	3	Water cycle for WAG B1 group in PD2
PD2WA2WATCYC	month	1	0	3	Water cycle for WAG B2 group in PD2
PD2WA3WATCYC	month	1	0	3	Water cycle for WAG B3 group in PD2
PD2WA4WATCYC	month	1	0	3	Water cycle for WAG B4 group in PD2
PD3WA1GASCYC	month	3	2	12	Gas cycle for WAG C1 group in PD3
PD3WA2GASCYC	month	5	2	12	Gas cycle for WAG C2 group in PD3
PD3WA3GASCYC	month	7	2	12	Gas cycle for WAG C3 group in PD3
PD3WA4GASCYC	month	9	2	12	Gas cycle for WAG C4 group in PD3
PD3WA1WATCYC	month	1	0	3	Water cycle for WAG C1 group in PD3
PD3WA2WATCYC	month	1	0	3	Water cycle for WAG C2 group in PD3
PD3WA3WATCYC	month	1	0	3	Water cycle for WAG C3 group in PD3
PD3WA4WATCYC	month	1	0	3	Water cycle for WAG C4 group in PD3
PD4WA1GASCYC	month	3	2	12	Gas cycle for WAG D1 group in PD4
PD4WA2GASCYC	month	5	2	12	Gas cycle for WAG D2 group in PD4
PD4WA3GASCYC	month	7	2	12	Gas cycle for WAG D3 group in PD4
PD4WA4GASCYC	month	9	2	12	Gas cycle for WAG D4 group in PD4
PD4WA1WATCYC	month	1	0	3	Water cycle for WAG D1 group in PD1
PD4WA2WATCYC	month	1	0	3	Water cycle for WAG D2 group in PD1
PD4WA3WATCYC	month	1	0	3	Water cycle for WAG D3 group in PD1
PD4WA4WATCYC	month	1	0	3	Water cycle for WAG D4 group in PD1

1

2

References

1. Dai, Z.; Viswanathan, H.; Middleton, R.; Pan, F.; Ampomah, W.; Yang, C.; Jia, W.; Xiao, T.; Lee, S.-Y.; McPherson, B., CO2 accounting and risk analysis for CO2 sequestration at enhanced oil recovery sites. *Environmental Science & Technology* **2016,** 50, (14), 7546-7554.

2. Ahmmed, B.; Appold, M. S.; Fan, T.; McPherson, B. J.; Grigg, R. B.; White, M. D., Chemical effects of carbon dioxide sequestration in the Upper Morrow Sandstone in the Farnsworth, Texas, hydrocarbon unit. *Environmental Geosciences* **2016,** 23, (2), 81-93.

3. White, M. D.; McPherson, B. J.; Grigg, R. B.; Ampomah, W.; Appold, M. S., Numerical simulation of carbon dioxide injection in the western section of the Farnsworth Unit. *Energy Procedia* **2014,** 63, 7891-7912.

4. Pan, F.; McPherson, B. J.; Dai, Z.; Jia, W.; Lee, S.-Y.; Ampomah, W.; Viswanathan, H.; Esser, R., Uncertainty analysis of carbon sequestration in an active CO 2-EOR field. *International Journal of Greenhouse Gas Control* **2016,** 51, 18-28.

5. Dai, Z.; Viswanathan, H.; Fessenden-Rahn, J.; Middleton, R.; Pan, F.; Jia, W.; Lee, S.-Y.; McPherson, B.; Ampomah, W.; Grigg, R., Uncertainty quantification for CO2 sequestration and enhanced oil recovery. *arXiv preprint arXiv:1411.4900* **2014**.

6. Ampomah, W.; Balch, R.; Grigg, R.; Will, R.; Dai, Z.; White, M. In *Farnsworth field CO 2-EOR project: performance case history*, SPE improved oil recovery conference, 2016; Society of Petroleum Engineers: 2016.

7. Amooie, M. A.; Soltanian, M. R.; Moortgat, J., Solutal convection in porous media: Comparison between boundary conditions of constant concentration and constant flux. *Physical Review E* **2018,** 98, (3), 033118.

8. Jia, W.; McPherson, B.; Pan, F.; Dai, Z.; Moodie, N.; Xiao, T., Impact of three-phase relative permeability and hysteresis models on forecasts of storage associated with CO2-EOR. *Water Resources Research* **2018,** 54, (2), 1109-1126.

9. Dai, Z.; Xu, L.; Xiao, T.; McPherson, B.; Zhang, X.; Zheng, L.; Dong, S.; Yang, Z.; Soltanian, M. R.; Yang, C., Reactive chemical transport simulations of geologic carbon sequestration: Methods and applications. *Earth-Science Reviews* **2020**, 103265.

10. Soltanian, M. R.; Hajirezaie, S.; Hosseini, S. A.; Dashtian, H.; Amooie, M. A.; Meyal, A.; Ershadnia, R.; Ampomah, W.; Islam, A.; Zhang, X., Multicomponent reactive transport of carbon dioxide in fluvial heterogeneous aquifers. *Journal of Natural Gas Science and Engineering* **2019,** 65, 212-223.

11. Ershadnia, R.; Wallace, C. D.; Soltanian, M. R., CO_2 geological sequestration in heterogeneous binary media: Effects of geological and operational conditions. *Advances in Geo-Energy Research* **2020,** 4, (4), 392-405.

12. Ershadnia, R.; Hajirezaie, S.; Amooie, A.; Wallace, C. D.; Gershenzon, N. I.; Hosseini, S. A.; Sturmer, D. M.; Ritzi, R. W.; Soltanian, M. R., CO2 geological sequestration in multiscale heterogeneous aquifers: Effects of heterogeneity, connectivity, impurity, and hysteresis. *Advances*

in Water Resources **2021,** 151, 103895.

13. Soltanian, M. R.; Amooie, M. A.; Cole, D. R.; Darrah, T. H.; Graham, D. E.; Pfiffner, S. M.; Phelps, T. J.; Moortgat, J., Impacts of methane on carbon dioxide storage in brine formations. *Groundwater* **2018,** 56, (2), 176-186.

14. Hoteit, H.; Fahs, M.; Soltanian, M. R., Assessment of CO2 injectivity during sequestration in depleted gas reservoirs. *Geosciences* **2019,** 9, (5), 199.

15. Guevara, J.; Ortega, A.; Canelón, J.; Nava, E.; Queipo, N. In *Model-Based Adaptive-Predictive Control and Optimization of SAGD under Uncertainty*, SPE Latin American and Caribbean Petroleum Engineering Conference, 2015; Society of Petroleum Engineers: 2015.

16. Forooghi, A.; Hamouda, A.; Eilertsen, T., Co-optimization of CO2 EOR and sequestration in a North Sea chalk reservoir. . In *EAGE Reservoir Charac-terization and Simulation Conference*, Abu Dhabi, UAE, 2009.

17. Han, Y.; Park, C.; Kang, J. M. In *Estimation of Future Production Performance Based on Multi-objective History Matching in a Waterflooding Project*, SPE EUROPEC/EAGE Annual Conference and Exhibition, 2010; Society of Petroleum Engineers: 2010.

18. Dai, Z.; Middleton, R.; Viswanathan, H.; Fessenden-Rahn, J.; Bauman, J.; Pawar, R.; Lee, S.-Y.; McPherson, B., An integrated framework for optimizing CO2 sequestration and enhanced oil recovery. *Environmental Science & Technology Letters* **2014,** 1, (1), 49-54.

19. You, J.; Ampomah, W.; Sun, Q.; Kutsienyo, E. J.; Balch, R. S.; Dai, Z.; Cather, M.; Zhang, X.,

Machine learning based co-optimization of carbon dioxide sequestration and oil recovery in CO2-EOR project. *Journal of Cleaner Production* **2020,** 260, 120866.

20. Omran, H.; El-Marsafy, S.; Ashour, F.; Abadir, E., Economic evaluation of aromatics production, a case study for financial model application in petrochemical projects. *Egyptian Journal of Petroleum* **2017,** 26, (4), 855-863.

21. You, J.; Ampomah, W.; Sun, Q., Development and application of a machine learning based multi-objective optimization workflow for CO2-EOR projects. *Fuel* **2020,** 264, 116758.

22. Wang, X.; van't Veld, K.; Marcy, P.; Huzurbazar, S.; Alvarado, V., Economic co-optimization of oil recovery and CO2 sequestration. *Applied Energy* **2018,** 222, 132-147.

23. Leach, A.; Mason, C. F.; van't Veld, K., Co-optimization of enhanced oil recovery and carbon sequestration. *Resource and Energy Economics* **2011,** 33, (4), 893-912.

24. Park, H.-Y.; Datta-Gupta, A.; King, M. J., Handling conflicting multiple objectives using Pareto-based evolutionary algorithm during history matching of reservoir performance. *Journal of Petroleum Science and Engineering* **2015,** 125, 48-66.

25. Rostamian, A.; Jamshidi, S.; Kamari, M. In *Non-Dominated Ranked Based Genetic Algorithm Multi-Objective Well Placement Optimization*, 81st EAGE Conference and Exhibition 2019, 2019; 2019.

26. Fonseca, R. M.; Reynolds, A. C.; Jansen, J. D., Generation of a Pareto front for a bi-objective

water flooding optimization problem using approximate ensemble gradients. *Journal of Petroleum Science and Engineering* **2016,** 147, 249-260.

27. Ampomah, W.; Balch, R. S.; Grigg, R. B.; McPherson, B.; Will, R. A.; Lee, S. Y.; Dai, Z.; Pan, F., Co-optimization of CO2-EOR and storage processes in mature oil reservoirs. *Greenhouse Gases: Science and Technology* **2017,** 7, (1), 128-142.

28. Ampomah, W.; Balch, R.; Cather, M.; Will, R.; Gunda, D.; Dai, Z.; Soltanian, M., Optimum design of CO 2 storage and oil recovery under geological uncertainty. *Applied Energy* **2017,** 195, 80-92.

29. He, L.; Huang, G.-h.; Zeng, G.-m.; Lu, H.-w., An integrated simulation, inference, and optimization method for identifying groundwater remediation strategies at petroleum-contaminated aquifers in western Canada. *Water Research* **2008,** 42, (10-11), 2629-2639.

30. Priezzhev, I.; Scollard, A.; Lu, Z., Regional production prediction technology based on gravity and magnetic data from the Eagle Ford formation. *Texas, USA, Denver SEG* **2014**.

31. El-Sebakhy, E. A.; Sheltami, T.; Al-Bokhitan, S. Y.; Shaaban, Y.; Raharja, P. D.; Khaeruzzaman, Y. In *Support vector machines framework for predicting the PVT properties of crude oil systems*, SPE Middle East Oil and Gas Show and Conference, 2007; Society of Petroleum Engineers: 2007.

32. Anderson, R. N. In *'Petroleum Analytics Learning Machine'for optimizing the Internet of*

Things of today's digital oil field-to-refinery petroleum system, 2017 IEEE International Conference on Big Data (Big Data), 2017; IEEE: 2017; pp 4542-4545.

33. Grimstad, B.; Foss, B.; Heddle, R.; Woodman, M., Global optimization of multiphase flow networks using spline surrogate models. *Computers & Chemical Engineering* **2016,** 84, 237-254.

34. Innocente, M. S.; Afonso, S. M. B.; Sienz, J.; Davies, H. M., Particle swarm algorithm with adaptive constraint handling and integrated surrogate model for the management of petroleum fields. *Applied Soft Computing* **2015,** 34, 463-484.

35. Caballero, J. A.; Grossmann, I. E., An algorithm for the use of surrogate models in modular flowsheet optimization. *AIChE journal* **2008,** 54, (10), 2633-2650.

36. Ampomah, W.; Balch, R.; Ross-Coss, D.; Hutton, A.; Cather, M.; Will, R. In *An integrated approach for characterizing a sandstone reservoir in the Anadarko Basin*, Offshore Technology Conference, 2016; Offshore Technology Conference: 2016.

37. Munson, T. W., Depositional, diagenetic, and production history of the Upper Morrowan Buckhaults Sandstone, Farnsworth Field, Ochiltree County Texas. **1994**.

38. Sun, Q.; Ampomah, W.; Kutsienyo, E. J.; Appold, M.; Adu-Gyamfi, B.; Dai, Z.; Soltanian, M. R., Assessment of CO2 trapping mechanisms in partially depleted oil-bearing sands. *Fuel* **2020,** 278, 118356.

39. Ampomah, W.; Balch, R.; Cather, M.; Rose-Coss, D.; Dai, Z.; Heath, J.; Dewers, T.; Mozley, P., Evaluation of CO2 storage mechanisms in CO2 enhanced oil recovery sites: Application to

Morrow sandstone reservoir. *Energy & Fuels* **2016,** 30, (10), 8545-8555.

40. Ross-Coss, D.; Ampomah, W.; Cather, M.; Balch, R.; Mozley, P.; Rasmussen, L. In *An improved approach for sandstone reservoir characterization*, SPE Western Regional Meeting, 2016; Society of Petroleum Engineers: 2016.

41. Gallagher, S. R. Depositional and diagenetic controls on reservoir heterogeneity: upper morrow sandstone, Farnsworth unit, Ochiltree county, Texas. Citeseer, 2014.

42. Rasmussen, L.; Fan, T.; Rinehart, A.; Luhmann, A.; Ampomah, W.; Dewers, T.; Heath, J.; Cather, M.; Grigg, R., Carbon Storage and Enhanced Oil Recovery in Pennsylvanian Morrow Formation Clastic Reservoirs: Controls on Oil–Brine and Oil–CO2 Relative Permeability from Diagenetic Heterogeneity and Evolving Wettability. *Energies* **2019,** 12, (19), 3663.

43. You, J. MULTI-OBJECTIVE OPTIMIZATION OF CARBON DIOXIDE ENHANCED OIL RECOVERY PROJECTS USING MACHINE LEARNING ALGORITHMS PhD Dissertation, New Mexico Institute of Mining and Technology, 2020.

44. Godec, M., Acquisition and Development of Selected Cost Data for Saline Storage and Enhanced Oil Recovery (EOR) Operations. *US National Energy Technology Laboratory. DOE/NETL-2014/1658* **2014**.

45. Suykens, J. A. K.; Gestel, T. V. G.; Brabanter, J. D.; Moor, B. D.; Vandewalle, J., *Least squares support vector machines*. World Scientific: 2002.

46. Snoek, J.; Larochelle, H.; Adams, R. P. In *Practical bayesian optimization of machine*

learning algorithms, Advances in neural information processing systems, 2012; 2012; pp 2951-2959.

47. Swersky, K.; Snoek, J.; Adams, R. P. In *Multi-task bayesian optimization*, Advances in neural information processing systems, 2013; 2013; pp 2004-2012.

48. Jarrell, P. M.; Fox, C. E.; Stein, M. H.; Webb, S. L., *Practical aspects of CO2 flooding*. Society of Petroleum Engineers Richardson, TX: 2002; Vol. 22.

49. Couet, B.; Djikpesse, H. A.; Tonkin, T.; Wilkinson, D. J. In *Production enhancement through integrated asset modeling optimization*, SPE production and operations conference and exhibition, 2010; Society of Petroleum Engineers: 2010.

50. Fan, J.-L.; Xu, M.; Yang, L.; Zhang, X.; Li, F., How can carbon capture utilization and storage be incentivized in China? A perspective based on the 45Q tax credit provisions. *Energy Policy* **2019,** 132, 1229-1240.